Fire Safety Journal 141 (2023) 104004

Contents lists available at ScienceDirect

Fire Safety Journal

journal homepage: www.elsevier.com/locate/firesaf

An empirical firebrand pile heat flux model

Jacques A. De Beer [a,*], Emily L. Dietz [a], Stanislav I. Stoliarov [a], Michael J. Gollner [b]

[a] Department of Fire Protection Engineering, University of Maryland, College Park, USA
[b] Department of Mechanical Engineering, University of California, Berkeley, USA

ARTICLE INFO

Keywords:
Wildland-urban interface fires
Glowing embers
Ignition of building materials
Thermal imaging
Inverse heat flux analysis

ABSTRACT

Firebrand exposure has been identified as a leading cause of structure losses during wildfires. However, only a limited number of studies have attempted to quantify the incident firebrand heat flux to a target substrate surface. In this study, a bench-scale wind tunnel retrofitted with an IR thermal imaging system was used to generate high-resolution temperature data for the back surface of a thin, non-combustible insulation board exposed to a glowing firebrand pile at 0.9–2.7 m s^{-1} air flow velocities and 0.06 and 0.16 g cm^{-2} firebrand coverage densities. An inverse heat flux modelling technique utilizing a solid-phase pyrolysis solver, ThermaKin, was employed to determine transient firebrand pile heat flux profiles underneath and directly in front of a glowing firebrand pile. The inverse modelling technique used both the experimental back surface temperature data and the insulation's thermophysical properties. Average incident firebrand pile heat flux values obtained for all testing conditions ranged between 28 and 80 kW m^{-2}. For the first time, an empirical model capturing the firebrand pile incident heat flux dependence on time, air flow velocity and firebrand coverage density was developed.

1. Introduction

Globally, the occurrence and impact of wildfires is on the rise. Three main mechanisms have been identified by which wildfires spread into the Wildland-Urban Interface (WUI): direct flame contact, radiation, and firebrand exposure [1]. Firebrand exposure has been linked to a large fraction of structure losses during WUI fires. Firebrands are hot embers generated and lofted from the combustion of vegetation or structural components which have the potential to ignite flammable target fuels kilometers downstream of the main fire front. Due to the significant impact of firebrand exposure, extensive research has been conducted in an effort to better understand the generation, transport, and ignition of substrates by firebrands. A number of reviews have indicated that a better understanding of the mechanisms responsible for the ignition of flammable target substrates by firebrands is still required [1–5].

Large- and bench-scale studies have evaluated the ignition of lignocellulosic substrates when exposed to a singular or a group of glowing firebrands. Firebrands that accumulate into groups have been found to increase the ignition susceptibility of target substrates [6,7]. Increased heat exposure from groups of firebrands to the surface of a target substrate has been identified as a key parameter affecting the substrate's ignition susceptibility. Previous studies have measured the heat exposure from firebrands onto the surface of a flat, horizontal target substrate using: a water-cooled heat flux gauge positioned underneath a group of artificial firebrands [8–10], an inverse heat flux analysis technique based on infrared (IR) thermal imaging of the back surface temperature of a thin stainless steel plate onto which a pile of artificial firebrands was deposited [11,12], and phosphor thermometry [13]. The firebrand pile heat exposure dependence on firebrand pile size and forced air flow velocity was evaluated in these heat transfer studies. Some of the main finding included the firebrand pile peak heat flux plateauing as the firebrand pile size was increased above 8 g, with pile heat flux averages reaching upwards of 50 kW m^{-2} and the firebrand pile heat flux continually increasing over the range of forced air flows studied (0–2.0 m s^{-1}). Mean firebrand surface temperatures were also measured [13–15] and were found to range from 500 K to 1223 K depending on forced air flow conditions (1 m s^{-1} – 4 m s^{-1}). Recent studies have also highlighted the dominant role of radiation from a firebrand pile in the ignition of a lignocellulosic material's surface located near the pile [16].

Quantifying the incident heat exposure from a group of firebrands onto the surface of a flammable target substrate for a range of air flows and firebrands pile sizes, representative of real wildfire events, is crucial when predicting the ignition susceptibility of a flammable target

* Corresponding author.
E-mail address: jdebeer@umd.edu (J.A. De Beer).

https://doi.org/10.1016/j.firesaf.2023.104004
Received 21 June 2023; Accepted 23 September 2023
Available online 23 September 2023

substrate by firebrands. In the current study, bench scale wind tunnel experiments were performed to generate Oriented Strand Board (OSB) ignition statistics and glowing-firebrand-pile-exposed substrate back surface temperature data for a range of air flows and firebrand pile sizes. A thin (0.318 cm thick) layer of Kaowool PM, which is a non-combustible insulation material, was used as an inert target substrate onto which a pile of glowing firebrands was deposited. IR thermal imaging was used to collect transient Kaowool PM back surface temperature data which in turn was used to inversely model the incident heat flux from a glowing firebrand pile onto a target substrate using a solid-phase pyrolysis solver, ThermaKin [17]. A set of conical radiant heater experiments was preformed to verify the accuracy of the Kaowool PM thermophysical properties, which are required as ThermaKin inputs when inversely modelling the firebrand pile heat fluxes. For the first time, an empirical model capturing the transient firebrand pile incident heat flux dependence on forced air flow velocity and firebrand pile coverage density has been developed. The results of this study will enable transient firebrand pile heat flux exposure predictions over a range of forced air flows and firebrand pile sizes, which can assist future modelling efforts seeking to predict the ignition of flammable target substrates by a pile of glowing firebrands.

2. Experimental

2.1. Bench-scale wind tunnel apparatus

The bench-scale wind tunnel used in this study is shown in Fig. 1 (a). The wind tunnel is comprised of three main sections: the contraction cone, the test section, and the exhaust. A honeycomb inset along with several mesh screens are installed along the length of the contraction cone and are used to straighten and laminarize the air flow into the test section. A flat, horizontal sample substrate can be mounted in the center of the test section using a detachable sample holder such that the top surface of the sample is flush with the bottom interior wall of the test section. The sample holder was constructed such that the bottom surface of the sample substrate was exposed. Glowing firebrands were deposited in the center of the sample substrate's top surface using a custom-built funnel. The funnel ensured that a constant 50 cm^2 (5 cm × 10 cm) firebrand pile deposition area was maintained for all tests.

The sample substrate back surface temperature was measured using a thermal imaging system shown in Fig. 1 (b). The thermal imaging system included an IR FLIR E95 thermal imaging camera and a square gold mirror. The gold mirror was used to redirect the view of the IR camera to the bottom surface of the sample substrate. The transient back surface temperature of a sample substrate was obtained from 464 × 384 pixel resolution thermal images. Two cutouts along the side and top wall of the test section are lined with borosilicate glass and provide optical access to the top surface of the substrate onto which glowing firebrands are deposited. The cutouts are used for visual identification of ignitions events which are recorded using two DSLR cameras. A high-temperature booster fan which was connected to a fan speed adjuster was used to control the air flow velocity within the test section over a range of 0–2.9 m s^{-1}. An Omega HHF-SD1 hot wire anemometer was used to verify the air flow velocity within the test section before the start of each test. A detailed description of each of the bench-scale wind tunnel components has been outlined in an earlier study [16].

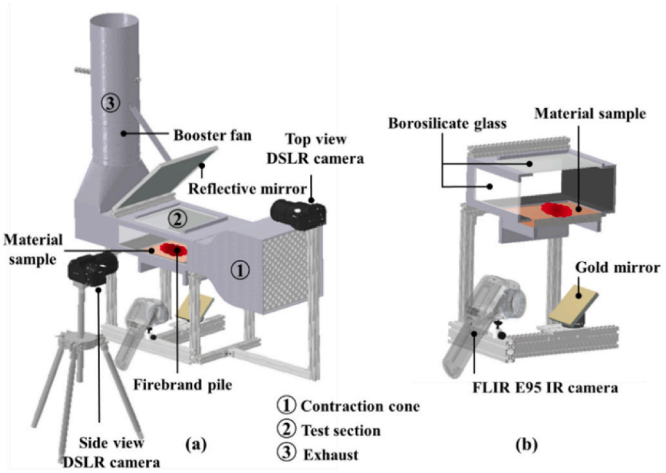

Fig. 1. (a) Bench-scale wind tunnel setup drawn to scale; (b) the thermal imaging portion of the wind tunnel setup.

2.2. Glowing firebrand piles

All firebrands used in this study were generated using 6.35 mm outer diameter and 25.4 mm long oven-dried artificial birch wood cylindrical dowels. The glowing firebrands were prepared using a procedure outlined in Ref. [16] which involves igniting a pile of dowels over a propane burner followed by extinguishing the burner and allowing the ignited dowels to transition to glowing firebrands. This process produces glowing firebrands with sizes representative of firebrands from actual wildfire events [18]. The mean mass and projected area, assuming a rectangular shape, of a single glowing firebrand from this study was 44.5 ± 10.8 mg and 0.63 ± 0.11 cm^2, respectively. Two different firebrand pile sizes were used in this study and were characterized by a coverage density. The firebrand pile coverage density (expressed in g cm^{-2}) was defined as the mass of glowing firebrands at the start of the experiment per unit area of the surface they were deposited on (50 cm^2). The two firebrand pile coverage densities used in this study were equal to 0.06 g cm^{-2} and 0.16 g cm^{-2}. The 0.06 g cm^{-2} firebrand pile corresponded to a single layer of firebrands (approximately 7 mm in height) deposited onto the surface of a test substrate. The 0.16 g cm^{-2} firebrand pile (about 20 mm in height) corresponded to the maximum pile size that could be maintained on a flat horizontal surface at the maximum forced air flow velocity (2.7 m s^{-1}) employed in this study.

2.3. Target substrates

Two materials were used in the current study: a 1.2 cm thick Georgia-Pacific Blue Ribbon PS2-10-compliant Oriented Strand Board (OSB) board, and a 0.318 cm thick Kaowool PM ceramic fiber insulation board. OSB is a dense engineered wood frequently used as a wall lining and roof covering material. Another lignocellulosic building material, Western Red Cedar (WRC), was studied in the same setup in an earlier work [16]. OSB and WRC have significantly different mass densities. A comparative analysis of these materials is expected to reveal how density impacts the ignition propensity.

All the target substrates were machined into 0.185 m × 0.145 m (in length and width) rectangles with the length of the sample positioned parallel with the direction of the incoming forced air flow into the wind tunnel. An 80 cm^2 section of the back surface of all the samples was painted with a MedTherm optical black coating with a broadband emissivity of 0.94. This section included the 50 cm^2 firebrand pile deposition area. The back surface of each sample was painted with the optical black coating to ensure accurate back surface temperature readings using the IR thermal imaging camera. For all tests, the 5 cm length of the firebrand pile was positioned perpendicular with the direction of the incoming air flow. All OSB samples (moisture content equal to 7 wt% dry basis) were conditions in a desiccator maintained at 21–23 °C and a relative humidity of 20–25% for at least 48 h prior to testing.

2.4. Testing matrix and procedure

Nine repeat tests were performed for each target substrate and each testing condition combination, which included four forced air flow

velocities ranging from 0.9 to 2.7 m s^{-1} and two different firebrand pile coverage densities. Each of the experiments in this study was performed in the bench-scale wind tunnel using the same testing procedure. Before the beginning of an experiment, the target substrate was mounted within the test section of the wind tunnel and the air flow was set. The predetermined mass of dowels was exposed to a propane flame for 40 s and was then left to transition to glowing firebrands. The recordings for the IR thermal imaging camera as well as both DSLR camera were initiated during the dowel-firebrand transitioning period. The dowel-firebrand transition was complete when no visible flames could be observed over the firebrand pile. The glowing firebrands were deposited onto the top surface of the target substrate, within 5 s after the transition was completed, using a custom-built funnel. Once the glowing firebrands were deposited, the funnel was removed, and a piece of borosilicate glass was used to seal the tunnel. The time at which the tunnel was sealed was taken as the official test start time for the purpose of analysis.

3. Some key results and their analysis

3.1. Flame ignitions

During preliminary analysis of the DSLR video recordings collected in the wind tunnel experiments, two distinct flaming ignition events were identified: the ignition of the firebrand pile, which was observed in Kaowool PM and OSB experiments, and the ignition of the flammable substrate surface, which was observed only in the OSB experiments. The flammable substrate surface ignition event was identified by the presence of an amber, diffusion-like flame attached to the surface of the substrate. The surface ignition event was more likely to lead to fire growth due to direct engagement of the flammable substrate and, therefore, was the main target of the current study. Representative snapshots of a flammable substrate surface ignition event are shown in Fig. 2.

A map of OSB surface ignitions summarizing observations at all testing conditions is shown in Fig. 3 (a). In this map, the number of surface ignitions is represented by three distinct areas: the area where no (or 0) ignitions was observed, the area where one (1) ignition was observed, and the area where two or more (2+) ignitions were observed. As this data indicates, an overwhelming majority of the OSB surface ignitions originate in front of the air flow-facing edge of the firebrand pile. This ignition location observation is consistent with the results obtained in an earlier study for WRC [16]. The prevalence of this location can be explained by a combination of high radiative heat flux from the adjacent wind-facing edge of the pile inducing pyrolysis of the flammable substrate and the availability of oxygen delivered by the incoming air flow. The glowing firebrands located at the very edge of the pile are likely to serve as a pilot for ignition of the pyrolyzates.

Fig. 3 (b) summarizes the observed dependence of the OSB surface ignition probability on air flow velocity at a 0.16 g cm^{-2} firebrand pile density. No OSB surface ignitions were observed at the 0.06 g cm^{-2} firebrand pile density. The ignition probability was calculated as the number of tests where an ignition took place divided by the total number of tests (9) performed at a given set of conditions. The highest ignition probability is observed at the 2.4 m s^{-1} air flow velocity. Further increases in the air flow causes the ignition probability to decrease. A similar trend in the ignition probability was observed in an earlier study of WRC [16]. This decrease is likely to be associated with a slight decrease in the radiative heat flux from the glowing firebrands (analyzed in detail in Section 4) and a decrease in the stability of the diffusion flame at higher air flow velocities (blow off effect [19]).

3.2. Kaowool PM insulation back surface temperature measurements

The thermal exposure from a firebrand pile onto the surface of a target substrate was isolated using non-combustible Kaowool PM insulation board. Kaowool PM has a low thermal conductivity and heat capacity (see Table 1) making its interference with the firebrand combustion process minimal. The Kaowool PM samples were also sufficiently thin (3.18 mm) to allow for accurate tracking of the temporal evolution of the firebrand pile thermal exposure via non-contact back surface temperature measurements. The mean density for Kaowool PM was calculated in-house using mass and volume measurements of ten 0.1 × 0.1 m^2 Kaowool PM samples (3.18 mm thick).

For this study, Kaowool PM back surface temperature data was generated for two measurement zones along the length of the pile as shown in Fig. 4. The preleading zone (zone 1) was located at the air flow facing edge of the firebrand pile and was 1.5 cm long. This zone extended 1 cm outside of the air flow-facing edge of the firebrand pile deposition area. As indicated in Section 3.1, an overwhelming majority of flammable substrate surface ignitions originated in front of the pile which corresponds to the preleading temperature measurement zone. The leading zone (zone 2) was 3 cm in length and was located underneath the firebrand pile and directly behind the preleading zone. The leading zone was analyzed here because this is where the highest substrate temperature was observed. Both zones were 4 cm wide, which is slightly lower than the total width of the firebrand pile.

As the data in Fig. 4 indicates, the back surface temperature varied significantly in space and time. To capture the main trends, the mean back surface temperature and spatial temperature variation within each zone was computed by using 30 and 24 spot measurements for the leading and preleading zone respectively. The spot measurements were distributed randomly within each zone and no preference was given to hot or cold areas. Each spot measurement contains 9 pixels which equates to nine individual temperature measurements. Nine repeat tests were used to compute a single time-resolved average back surface temperature profile for each testing condition combination. The spatial and test-to-test temperature variation at each time step was calculated as two standard deviations. Preleading and leading zone Kaowool PM back surface temperature profiles for all testing conditions are presented in Section 1 of the supplementary materials.

4. Firebrand pile inverse heat flux modelling

The Kaowool PM back surface temperature data can be used as a surrogate measurement to quantify the firebrand pile thermal exposure dependence on the air flow velocity and firebrand pile coverage density. However, knowledge of the incident firebrand pile heat flux onto a target substrate surface is necessary to enable prediction of the ignition

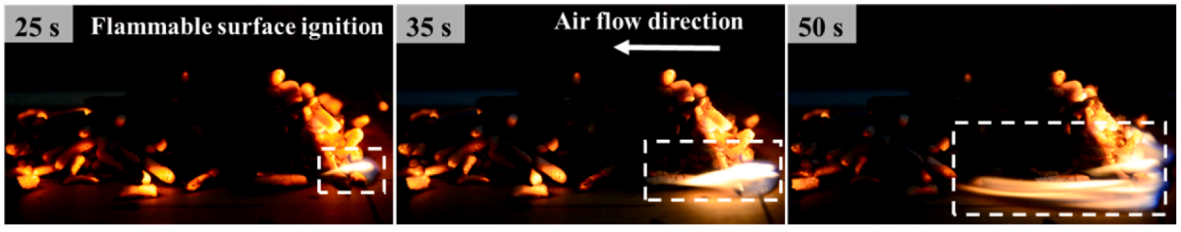

Fig. 2. Time-stamped side-view images of a flammable substrate surface ignition observed at 0.16 g cm^{-2} firebrand pile coverage density and 2.4 m s^{-1} air flow velocity. The dashed-line rectangle indicates the location of the flame attached to the substrate surface.

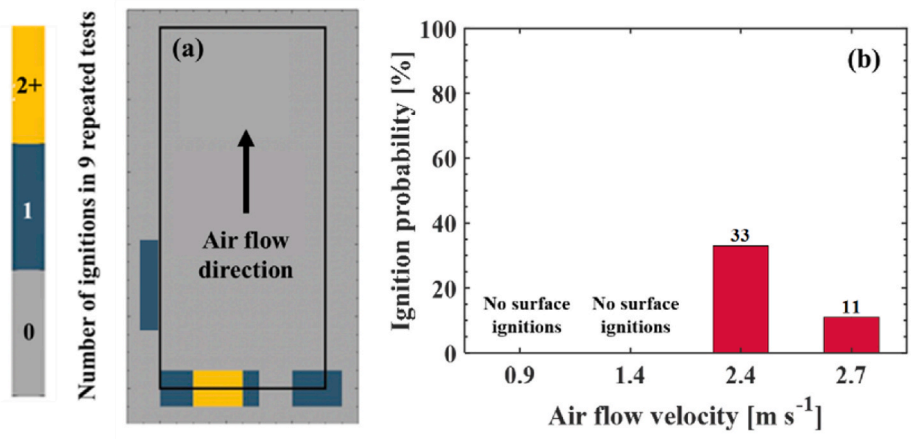

Fig. 3. (a) OSB surface ignition location map drawn to scale. The solid rectangle shows the boundaries of the 50 cm^2 firebrand pile deposition area. (b) OSB surface ignition probability computed from experiments performed at a 0.16 g cm^{-2} firebrand pile coverage density.

Table 1
Thermophysical properties of Kaowool PM insulation.

Material	Density ($kg\ m^{-3}$)	Heat Capacity ($J\ g^{-1}\ K^{-1}$)	Thermal Conductivity ($W\ m^{-1}\ K^{-1}$)
Kaowool PM	232	1.07 [20]	$0.049 + 1.5 \times 10^{-5}\,T + 1 \times 10^{-7}\,T^2$ (T in °C) [20]

of flammable substrates when exposed to a pile of glowing firebrands. The heat flux from a glowing firebrand pile to the surface of a target substrate was determined in this work using an inverse modelling technique which relied on a solid-phase pyrolysis solver, ThermaKin [17]. ThermaKin was selected because of the familiarity of the authors with this modelling tool. Generally, any one-dimensional heat transfer solver with flexible boundary conditions and temperature-dependent properties could be used in this exercise.

The inverse heat flux modelling procedure consisted of matching a ThermaKin-generated Kaowool PM back surface temperature temporal profile with the target average experimental back surface temperature profile by iteratively changing the incident heat flux temporal dependence specified in the model. This inverse modelling required the knowledge of relevant Kaowool PM thermophysical properties summarized in Table 1, emissivity of the Kaowool PM surface, and all boundary conditions with the exception of the incident firebrand pile heat flux. This inverse modelling approach concurs with several other studies [21,22] that show that more than one system measurement is required when determining the heat flux from temperature measurements.

4.1. Validation of Kaowool PM thermophysical properties

The inverse heat flux modelling requires an accurate definition of the properties that control heat transport inside the Kaowool PM board. Therefore, validation experiments and analysis were carried out to ensure that the properties listed in Table 1, which were originally provided by the manufacturer of this board, are valid. Three experiments were performed where the 3.18 mm thick Kaowool PM insulation board (used in the firebrand pile wind tunnel experiments) was placed on the top of a 25.4 mm thick Kaowool PM insulation slab and subjected to controlled radiative heat flux from a conical radiant heater similar to that used in a cone calorimeter [23]. Three K-type thermocouples (0.25 mm wire diameter) were placed in between the 3.18 mm thick Kaowool PM board and the 25.4 mm Kaowool PM slab and were used for in-depth transient temperature measurements. The thermocouples were positioned in the center of the Kaowool PM board. The radiant heater was set to deliver 50 kW m^{-2} of incident radiant heat flux to the top surface of the Kaowool PM board. This heat flux was set using a NIST-traceable calibrated Schmidt-Boelter water-cooled heat flux gauge. The top surface of the board (facing the radiant heater) was painted with a Med-Therm optical black coating with a broadband emissivity of 0.94.

The ThermaKin simulation of this radiative heating experiment was carried out using the Kaowool PM properties listed in Table 1 and emissivity of the radiation-exposed surface defined by the optical black coating (0.94). Natural convective losses from the top surface were taken into account using a convective heat transfer coefficient of 3.7 W $m^{-2}\ K^{-1}$ [24] (corresponding to the center of a 10 × 10 cm^2 sample) and an ambient temperature of 293 K. A 0.01 s time step and 5 × 10^{-5} m element size was used for the numerical integration. Increasing or decreasing these parameters by a factor of two did not change the results indicating convergence. The same integration parameters were used in all wind tunnel experiment simulations discussed in subsequent sections. In-depth radiation absorption was assumed negligible. The mean in-depth experimental temperature history (average of all thermocouple signals collected in 3 repeated tests) and the ThermaKin-simulated temperature history below the 3.18 mm thick painted Kaowool PM

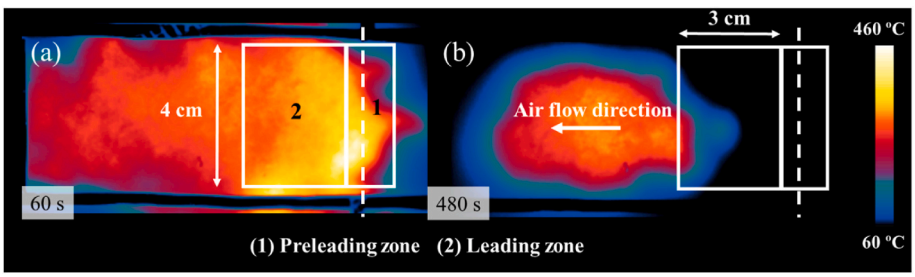

Fig. 4. Kaowool PM back surface temperature maps obtained for a 0.16 g cm^{-2} firebrand pile density and a 2.4 m s^{-1} air flow velocity at (a) 60 s and (b) 480 s after the start of the test. The airflow-facing edge of the firebrand pile is marked by the dashed line.

insulation board are compared in Fig. 5 (a). This comparison shows an excellent agreement between the experiments and the simulation confirming the validity of the Kaowool PM thermophysical properties, as listed in Table 1.

4.2. Modelling setup and procedure

The main assumption that was used in the inverse modelling of the heat flux from the firebrand pile was that, for both the preleading and leading zones, this heat flux was purely radiative in nature. Preliminary simulations indicated that the Kaowool PM back surface temperature data collected in the wind tunnel experiments can only be captured when this heat flux is defined as a time dependent function. A range of piecewise linear functions of various levels of complexity was examined and it was determined that the simplest function that captures all temperature data consists of three linear segments and has the shape shown in Fig. 5 (b). This shape, which consists of a rapid rise followed by a slower decay, mimics the shape of the firebrand pile burning rate dependence on time measured in an earlier study [16]. The rise is associated with an increase in the intensity of smoldering due to the exposure of the deposited firebrand pile to a forced air flow at the start of the experiment. The decay is associated with the consumption of firebrands.

The parameters that define the function shown in Fig. 5 (b) include the heat flux rise rate, HF_{Rise} (kW m^{-2} s^{-1}), the heat flux at the start of the test, $HF_{t\,=\,0}$ (kW m^{-2}), computed by multiplying HF_{Rise} by the time between the firebrand deposition and sealing of the tunnel (12 s), the time to the peak heat flux, t_{Rise} (s), the heat flux decay rate, HF_{Decay} (kW m^{-2} s^{-1}), the final constant heat flux, HF_{Final} (kW m^{-2}), and the time of decay from the peak to the final constant heat flux, t_{Decay} (s). Note that, just like $HF_{t\,=\,0}$, t_{Decay} is a dependent parameter that can be computed from HF_{Rise}, t_{Rise}, HF_{Decay}, and HF_{Final}.

The convective losses from the Kaowool PM board used in the wind tunnel experiments were defined as follows. The convective losses from the leading zone of the top surface were assumed to be negligible because, in this zone, the substrate was completely covered by firebrands. The convective losses from the top surface of the preleading zone were computed using well-known local forced flow correlations [25]. These correlations are summarized by Eqns. (1) and (2), where $h_{c,local}$ (W m^{-2} K^{-1}) is a local convective heat transfer coefficient, which is believed to provide a more accurate representation of the heat losses in the preleading zone than a global convection coefficient, which averages heat losses over the full length of the boundary layer.

$$h_{c,local} = \left(Nu_{local}\, k_{forced}\right) / L_{local} \tag{1}$$

$$Nu_{local} = 0.332 Re_{local}^{1/2} Pr^{1/3} \ \text{ for } \left(Re_{local} < 5\times 10^{5}, Pr \geq 0.6\right) \tag{2}$$

In Eqns. (1) and (2), L_{local} is the characteristic length, which was equated to be the distance from the entrance of the test section of the wind tunnel to the middle of the preleading zone, 0.125 m Re_{local}, Nu_{local}, and Pr are Reynolds, Nusselt and Prandtl numbers, respectively. k_{forced} is the thermal conductivity. All these quantities were computed assuming that the fluid is air at a film temperature of 493 K. This film temperature was determined as the mean of the ambient temperature of 293 K and the average substrate surface temperature measured underneath a pile of firebrands, 693 K [9,26]. $h_{c,local}$ was found to be equal to 5.1, 6.3, 8.3 and 8.8 W m^{-2} K^{-1} for 0.9, 1.4, 2.4 and 2.7 m s^{-1} air flow velocities, respectively.

The convective losses from the bottom surface of the Kaowool PM board were defined using the natural convection correlations obtained from Ref. [25] and summarized by Eqns. (3) and (4).

$$h_{free} = \left(Nu_{free}\, k_{free}\right) / L_{free} \tag{3}$$

$$Nu_{free} = 0.27 Ra_{free}^{1/4} \text{ for } \left(10^{5} \leq Ra_{free} < 10^{11}\right) \tag{4}$$

In these equations, h_{free} is the convection coefficient. L_{free} is the characteristic length set to 0.073 m, which is approximately half of the width of the Kaowool PM board. Nu_{free}, Ra_{free}, and k_{free} are the Nusselt number, Raleigh number and thermal conductivity, respectively. These quantities were computed for air at the film temperature of 433 K. This film temperature was determined as the mean of the ambient temperature (293 K) and the average Kaowool PM board back surface temperature measured in the tunnel experiments, 573 K. h_{free} was found to be equal to 4.8 W m^{-2} K^{-1}.

The final parameters required for the simulation of the Kaowool PM back surface temperature data collected in the wind tunnel experiments were the insulation board surface emissivities. The bottom surfaces of the Kaowool PM boards used in these experiments were painted with the MedTherm optical black coating and thus their emissivity was defined by the emissivity of the coating (0.94). The same approach could not be used for the top surface of Kaowool PM located underneath the firebrand pile because of a rapid thermal degradation of the coating when in direct contact with the glowing firebrands. To address this issue, additional experiments and analysis were carried out to determine the emissivity of unpainted Kaowool PM board.

First, a set of nine wind tunnel experiments was performed with both Kaowool PM board surfaces painted with the MedTherm coating. These

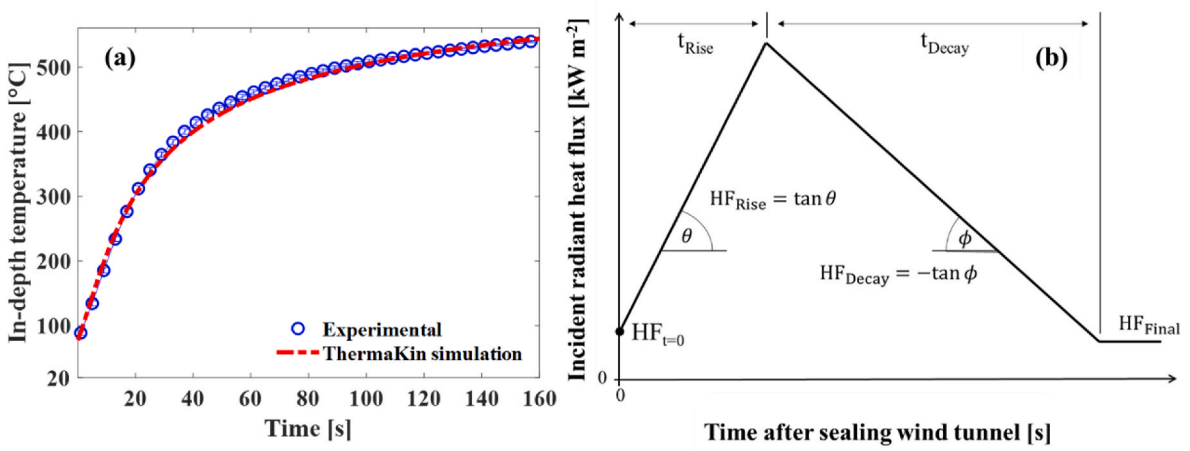

Fig. 5. (a) A comparison of the experimental and simulated in-depth (3.18 mm) temperature histories inside the Kaowool PM assembly exposed to 50 kW m^{-2} of incident radiant heat flux. (b) The dependence of incident radiant heat flux on time used in this work to represent the heat feedback from a firebrand pile to the target substrate surface.

tests were conducted at 2.4 m s^{-1} forced air flow velocity and 0.16 g cm^{-2} firebrand pile coverage density. Subsequently, the preleading zone back surface temperature data collected in these tests were subjected to the inverse heat flux modelling. These test results were deemed suitable for the modelling because both Kaowool PM surface emissivities were defined by the coating and the coating remained relatively intact in the preleading zone, which contained few firebrands.

During this modelling process, the parameters of the heat flux profile shown in Fig. 5 (b) were changed in small increments until the simulated Kaowool PM back surface temperature was found to capture the first 200 s of the mean experimental data with the coefficient of determination, R^2, higher than 0.96, as shown Fig. 6 (a). The time period was limited to 200 s because all OSB and WRC [16] surface flames extinguished prior to its end. The heat flux parameters obtained as the result of this exercise are summarized in Table 2. The uniqueness of these parameters was established by demonstrating, through exhaustive trial-and-error, that no other set of parameters could achieve the same level of agreement with the experimental data. Note that the experimental back surface temperature data exhibits a significant variation. This variation (expressed as two standard deviations) reflects primarily spatial variability in the thermal exposure associated with a discrete nature of the firebrand particles and changes in the exact spatial arrangement of these particles from test to test.

At the next step, a comparison was made between the experimental preleading zone back surface temperature histories obtained under the same experimental conditions, 2.4 m s^{-1} air flow and 0.16 g cm^{-2} firebrand coverage density, using Kaowool PM boards with unpainted and painted top surfaces. This comparison is provided in Fig. 6 (b). It indicates that the emissivity of the unpainted Kaowool PM surface is lower than that of the surface painted with the MedTherm optical black coating. Therefore, in the final step of this analysis, the unpainted Kaowool PM surface temperature data were used as a target for inverse modelling to determine the unpainted surface emissivity. This modelling relied on the knowledge of the firebrand incident heat flux profile, which parameters are summarized in Table 2, and the assumption that this profile is unaffected by the presence of the paint on the top surface of the Kaowool PM board. The emissivity values were adjusted in 0.01 increments until the best agreement between the experimental and simulated temperature profiles was achieved. This agreement is shown in Fig. 7. It was obtained using a Kaowool PM surface emissivity value of 0.64.

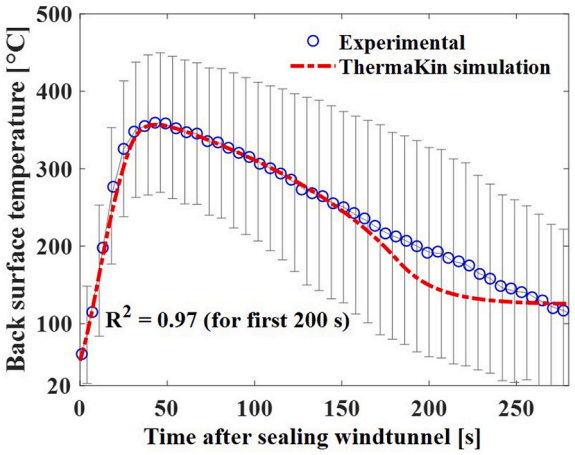

Fig. 7. Experimental and simulated back surface temperature histories obtained for the preleading zone of the Kaowool PM board with an unpainted top surface at a 2.4 m s^{-1} air flow velocity and a 0.16 g cm^{-2} firebrand pile coverage density.

4.3. Modelling results

Using the value of surface emissivity obtained for the unpainted Kaowool PM board, the preleading and leading zone back surface temperature data collected in the experiments at different air flow velocities and firebrand pile densities were analyzed to determine the corresponding parameters of the heat flux profiles. The same approach that was used to obtain the heat flux profile parameters for the preleading zone at 2.4 m s^{-1} air flow velocity and 0.16 g cm^{-2} firebrand pile coverage density discussed in Section 4.2 was followed. Table 3 summarizes the results of this exercise obtained for the preleading zone. A graphical representation of these profiles is given in Fig. 8. The corresponding leading zone results are provided in Section 3 of the supplementary materials.

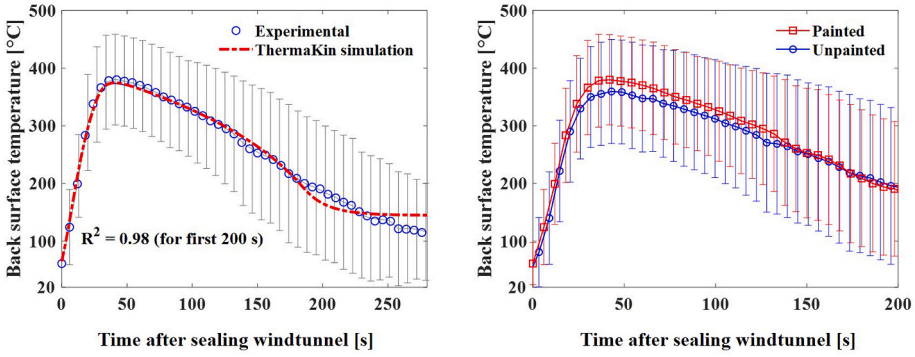

Fig. 6. (a) Experimental and simulated Kaowool PM back surface temperature histories obtained for the preleading zone at 2.4 m s^{-1} air flow velocity and 0.16 g cm^{-2} firebrand pile coverage density. The top surface of the preleading zone was painted with the MedTherm optical black coating. (b) A comparison of the experimental preleading zone back surface temperature histories obtained under the same conditions (2.4 m s^{-1} air flow and 0.16 g cm^{-2} firebrand density) using painted and unpainted Kaowool PM top surfaces.

Table 2
Parameters of the firebrand heat flux dependence on time obtained for the preleading zone at a 2.4 m s^{-1} air flow velocity and a 0.16 g cm^{-2} firebrand pile coverage density.

Test condition	$HF_{t=0}$ (kW m^{-2})	HF_{Rise} (kW m^{-2} s^{-1})	t_{Rise} (s)	HF_{Decay} (kW m^{-2} s^{-1})	t_{Decay} (s)	HF_{Final} (kW m^{-2})
2.4 m s^{-1}, 0.16 g cm^{-2}	26	2.15	39	−0.50	152	8

Table 3
Parameters of the firebrand heat flux dependences on time obtained for the preleading zone for all test conditions studied.

Test condition	$HF_{t=0}$ (kW m^{-2})	HF_{Rise} (kW m^{-2} s^{-1})	t_{Rise} (s)	HF_{Decay} (kW m^{-2} s^{-1})	t_{Decay} (s)	HF_{Final} (kW m^{-2})
0.9 m s^{-1}, 0.16 g cm^{-2}	14	1.20	42	−0.13	329	8
1.4 m s^{-1}, 0.16 g cm^{-2}	19	1.56	41	−0.25	225	8
2.4 m s^{-1}, 0.16 g cm^{-2}	26	2.15	39	−0.50	153	8
2.7 m s^{-1}, 0.16 g cm^{-2}	23	1.90	37	−0.52	120	8
1.4 m s^{-1}, 0.06 g cm^{-2}	11	0.95	41	−0.23	149	5
2.4 m s^{-1}, 0.06 g cm^{-2}	15	1.19	39	−0.42	99	5

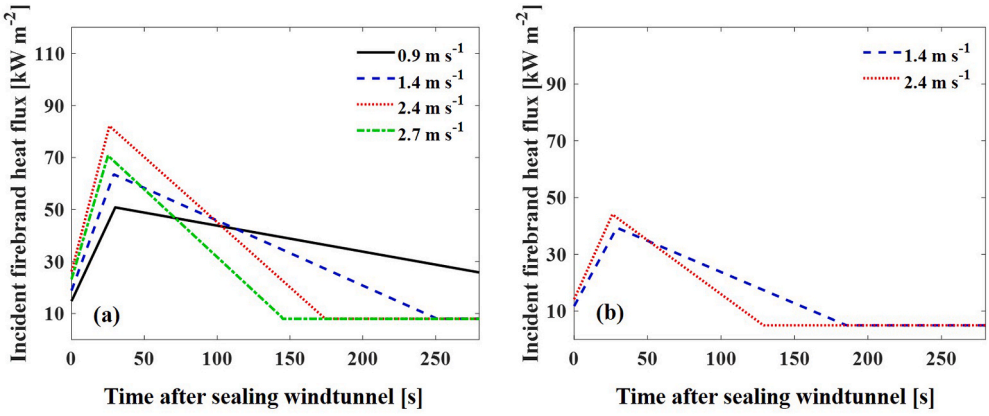

Fig. 8. Firebrand heat flux dependences on time obtained for the preleading zone at (a) 0.16 g cm^{-2} and (b) 0.06 g cm^{-2} firebrand pile coverage density.

Additional inverse modelling was performed to estimate the variation in the firebrand heat flux that produces the variation in the Kaowool PM back surface temperature measured in the experiments. It was found that, on average (for all testing conditions and both zones) the experimentally observed variation in temperature corresponds to ±40% variation in the heat flux. As was already pointed out, this variation is a consequence of the discrete nature of the firebrand particles and stochasticity of the deposition process, which is also an attribute of conditions encountered in real WUI fires.

4.4. Comparison with previous studies

In previous firebrand pile thermal exposure studies [8–12] a time-averaged heat flux from a firebrand pile to the surface of a target substrate was used as a measure of intensity of the firebrand pile thermal exposure. To enable comparison of the current results with these studies, average incident firebrand pile heat flux values for all testing conditions and both temperature measurement zones were computed from the modelled heat flux time dependencies. The average heat fluxes were calculated over a 100 s time frame, starting once the wind tunnel was sealed, and are provided in Table 4. The 100 s time frame was selected because all OSB and WRC [16] surface flame ignitions occurred within this time period.

Hakes et al. [8] and Salehizadeh et al. [9] measured the incident heat flux from a firebrand pile deposited on a horizontal inert substrate using a water-cooled Schmidt-Boelter heat flux gauge located directly underneath the firebrand pile. The average firebrand pile heat flux measured by Hakes et al. [8] over the first 100 s of the test using a constant forced air flow of 1.84 m s^{-1} and a pile mass of 5–9 g was approximately 20 kW m^{-2}. The average firebrand pile heat fluxes measured by Salehizadeh et al. [9] for air flows ranging between 0.5 and 2 m s^{-1} and 16 g firebrand pile were found to vary between 12 and 30 kW m^{-2}. A firebrand deposition area of 100 cm^2 was used by Salehizadeh et al. [9]. The averaged heat fluxes determined under similar conditions in the current study are significantly larger. This discrepancy is attributed to the fact that, unlike in the present study, Hakes et al. [8] and Salehizadeh et al. [9] measured their heat fluxes near the middle of the pile, which tends to be cooler than the leading and preleading zones [16]. The use of a water-cooled gauge by these researchers may have also affected the results of their measurements. A water-cooled heat flux gauge surface is likely to at least partially quench smoldering firebrands in the vicinity of this surface and thus reduce their heat feedback.

Bearinger et al. [11] measured the heat flux from a firebrand pile onto the surface of a thin horizontal stainless-steel plate onto which this pile was deposited using IR thermal imaging back surface temperature data and an inverse heat transfer technique. A 3 g firebrand pile, exposed to 2.0 m s^{-1} air flow, was deposited within a 20 cm^2 surface area of the steel plate, which produced a 0.15 g cm^{-2} coverage density. The resulting heat flux averaged over the same 100 s time period after the deposition of firebrands was found to be about 39 kW m^{-2}. This heat flux is closer to the current measurements (summarized in Table 4) but still about 40% lower at least partially due to the fact that Bearinger et al. [11] averaged their heat flux over the whole pile deposition area, whereas the current study focused on the hottest areas of the substrate defined by the preleading and leading zones [16].

Table 4
Incident heat flux values calculated from the modelled heat flux profiles by averaging the first 100 s of each time dependence.

Test condition	Preleading zone average heat flux (kW m^{-2})	Leading zone average heat flux (kW m^{-2})
0.9 m s^{-1}, 0.16 g cm^{-2}	38	43
1.4 m s^{-1}, 0.16 g cm^{-2}	46	53
2.4 m s^{-1}, 0.16 g cm^{-2}	58	80
2.7 m s^{-1}, 0.16 g cm^{-2}	47	69
1.4 m s^{-1}, 0.06 g cm^{-2}	28	35
2.4 m s^{-1}, 0.06 g cm^{-2}	30	44

Table 5
A set of functions that define the relation between the heat flux profile parameters obtained for the preleading zone, air flow velocity (v in m s^{-1}) and firebrand coverage density (ψ in g cm^{-2}).

Heat flux parameter	Correlation
$F(\psi)$	
$HF_{Rise\ rate}$, $HF_{Decay\ rate}$, HF_{Final}	$= \tanh(12 \times \psi)$
t_{Rise} (s)	$= 1$
Heat flux parameter ($\psi = 0.16$ g cm^{-2}, v)	
HF_{Rise} (kW m^{-2} s^{-1})	$= -0.29v^2 + 1.49v + 0.1$
t_{Rise} (s)	$= -0.58v^2 - 0.50v + 43$
HF_{Decay} (kW m^{-2} s^{-1})	$= -0.02v^2 - 0.13v - 0.01$
HF_{Final} (kW m^{-2})	$= 8$

5. A generalized relation between the firebrand pile heat flux, air flow velocity and pile density

At the final stage of this work, firebrand pile heat flux correlations were developed to capture the dependence of each heat flux parameter on forced air flow velocity and firebrand pile coverage density in the preleading and leading temperature measurement zones. These heat flux correlations were developed to allow interpolation of the heat flux parameters within the range of testing conditions and to enable potentially extrapolation of the heat flux parameters outside of the range of air flows and pile coverage densities studied. In this section, the firebrand pile coverage density is labeled as ψ (g cm^{-2}); and the forced air flow velocity as v (m s^{-1}).

The dependence of heat flux parameters on v was determined using the heat flux parameter values at $\psi = 0.16$ g cm^{-2} (given in Table 3). HF_{Final} was set to be independent on v. A second order polynomial was found to accurately represent the dependence of the rest of the heat flux parameters on air flow velocity. The graphs of the heat flux parameter values fitted with this second order polynomial function can be found in Section 4 of the supplementary materials.

The dependence on ψ was constructed by taking into account an observation of Hakes et al. [8] that increasing the firebrand pile mass above 8 g, which approximately corresponds to $\psi = 0.16$ g cm^{-2}, produced no significant changes in the heat flux to the horizontal substrate. The values of each heat flux parameter at each ψ and the same v were compared in an effort to capture each heat flux parameter's dependence on ψ. t_{Rise} was found to be independent of ψ. The rest of the heat flux parameters were normalized by the heat flux parameter value at $\psi = 0.16$ g cm^{-2} resulting in non-dimensional values that ranged from zero (at $\psi = 0$) to 1. These parameters were subsequently fitted with a hyperbolic tangent function, $F(\psi)$, which captures the limiting behavior of these parameters. In the final form, each independent heat flux parameter, including HF_{Rise}, t_{Rise}, HF_{Decay}, and HF_{Final}, was represented by the following function:

$$\text{Heat flux parameter}\,(\psi, v) = \text{Heat flux parameter}\left(\psi = 0.16\,\text{g cm}^{-2}, v\right) \times F(\psi) \tag{5}$$

The heat flux parameters of this function obtained for the preleading zone are provided in Table 5. The parameters determined for the leading zone can be found in Section 4 of the supplementary materials. To further verify these empirical correlations, they were used to generate heat flux profiles that were subsequently employed to simulate (with ThermaKin) experimental Kaowool PM back surface temperature histories for every set of conditions studied in this work. It was found that the preleading- and leading zone back surface temperature simulation results agree well with the experimental data yielding an average $R^2 = 0.92$ for all testing conditions studied. Each testing-condition specific R^2-value was calculated over the first 200 s of a test. The simulated peak-average back surface temperature values for the preleading and leading zone were within 10 and 19 °C of the experimental peak-average back surface temperature data, respectively. The peak–average back surface temperature was calculated over a 4 s time frame around the global peak back surface temperature value. Based on a general interpretation of the trends in the heat flux profile parameters, it was concluded that the developed preleading and leading zone heat flux parameter correlations should be applicable to a 0–4 m s^{-1} range of forced air flow velocities and any firebrand pile coverage density.

6. Conclusions

A bench-scale wind tunnel was employed to study heat feedback from a glowing firebrand pile to a horizontal substrate. The experiments were performed at forced air flow velocities ranging between 0.9 and 2.7 m s^{-1} and firebrand coverage densities of 0.06 and 0.16 g cm^{-2}. A combustible substrate, OSB, was studied to identify the areas of the substrate most susceptible to flame ignitions. A thin, non-combustible insulation board, Kaowool PM, was used as a substrate to quantify the intensity of the heat feedback through measurement of its back surface temperature.

Inverse modeling of this temperature in two specific zones, preleading and leading, located in front and underneath the pile, respectively, was used to obtain information on the incident heat flux from the firebrand pile to the substrate. The heat flux was assumed to be radiative in nature and dependent on time. A function consisting of three linear segments describing a rapid rise of the heat flux, associated with an application of forced air flow, followed by a slower decay, associated the consumption of the firebrands, was found to provide accurate predictions of the Kaowool PM back surface temperature. Parameters of this function were obtained for both preleading and leading zones and for every air flow velocity and firebrand pile coverage density studied. Average heat flux values, calculated over the first 100 s after application of forced air flow, were determined to range between 28 and 80 kW m^{-2}. The parameters of this function were subsequently correlated with forced air flow velocity and firebrand pile coverage density to enable both interpolation between experimentally studied conditions and extrapolation outside of this range of conditions. Based on a general interpretation of the trends in these parameters, the developed correlations should be applicable to a 0–4 m s^{-1} range of air flow velocities and any firebrand pile coverage density.

Author's contributions

Jacques A. De Beer – method development; data collection and analysis; manuscript writing.

Emily L. Dietz – data collection and analysis.

Stanislav I. Stoliarov – funding acquisition; conceptualization; method development; manuscript writing and editing.

Michael J. Gollner – funding acquisition; conceptualization; manuscript review.

Declaration of competing interest

The authors declare the following financial interests/personal relationships which may be considered as potential competing interests: Jacques A. De Beer reports financial support was provided by National Institute of Standards and Technology.

Data availability

Data will be made available on request.

Acknowledgements

This work was supported by the U.S. National Institute of Standards and Technology (NIST) grant number 70NANB19H053 and by a grant from the UL's Fire Safety Research Institute (FSRI). The authors are grateful to Dr. Gavin Horn of FSRI, Dr. Alexander Filkov of the University of Melbourne, and Dr. Peter Sunderland of the University of Maryland for insightful feedback and help with the logistics of this project.

Appendix A. Supplementary data

Supplementary data to this article can be found online at https://doi.org/10.1016/j.firesaf.2023.104004.

References

[1] S.E. Caton, R.S.P. Hakes, D.J. Gorham, A. Zhou, M.J. Gollner, Review of pathways for building fire spread in the wildland urban interface Part I: exposure conditions, Fire Technol. 53 (2) (2017) 429–473, https://doi.org/10.1007/s10694-016-0589-z.

[2] S. Nazare, I. Leventon, R. Davis, Ignitibility of Structural Wood Products Exposed to Embers during Wildland Fires: A Review of Literature, 2021, https://doi.org/10.6028/NIST.TN.2153.

[3] W.E. Mell, S.L. Manzello, A. Maranghides, D. Butry, R.G. Rehm, The wildland-urban interface fire problem - current approaches and research needs, Int. J. Wildland Fire 19 (2) (2010) 238–251, https://doi.org/10.1071/WF07131.

[4] A.C. Fernandez-Pello, Wildland fire spot ignition by sparks and firebrands, Fire Saf. J. 91 (2017) 2–10, https://doi.org/10.1016/j.firesaf.2017.04.040.

[5] S.L. Manzello, S. Suzuki, M.J. Gollner, A.C. Fernandez-Pello, Role of firebrand combustion in large outdoor fire spread, Prog. Energy Combust. Sci. 76 (2020), https://doi.org/10.1016/j.pecs.2019.100801.

[6] S.L. Manzello, S. Suzuki, Exposing decking assemblies to continuous wind-driven firebrand showers, Fire Saf. Sci. 11 (2014) 1339–1352.

[7] L.E. Hasburgh, D.S. Stone, S.L. Zelinka, Laboratory investigation of fire transfer from exterior wood decks to buildings in the wildland–urban interface, Fire Technol. 53 (2) (2017) 517–534, https://doi.org/10.1007/s10694-016-0588-0.

[8] R.S.P. Hakes, H. Salehizadeh, M.J. Weston-Dawkes, M.J. Gollner, Thermal characterization of firebrand piles, Fire Saf. J. 104 (2019) 34–42, https://doi.org/10.1016/j.firesaf.2018.10.002.

[9] H. Salehizadeh, R.S.P. Hakes, M.J. Gollner, Critical ignition conditions of wood by cylindrical firebrands, Front. Mech. Eng. 7 (2021), https://doi.org/10.3389/fmech.2021.630324.

[10] Z. Tao, B. Bathras, B. Kwon, B. Biallas, M.J. Gollner, R. Yang, Effect of firebrand size and geometry on heating from a smoldering pile under wind, Fire Saf. J. 120 (2021), https://doi.org/10.1016/j.firesaf.2020.103031.

[11] E. Bearinger, B.Y. Lattimer, J.L. Hodges, C. Rippe, A. Kapahi, Statistical assessment of parameters affecting firebrand pile heat transfer to surfaces, Front. Mech. Eng. 7 (2021), https://doi.org/10.3389/fmech.2021.702181.

[12] E.D. Bearinger, J.L. Hodges, F. Yang, C.M. Rippe, B.Y. Lattimer, Localized heat transfer from firebrands to surfaces, Fire Saf. J. 120 (2021), https://doi.org/10.1016/j.firesaf.2020.103037.

[13] Y.M. Abul-Huda, N. Bouvet, Thermal dynamics of deposited firebrands using phosphor thermometry, in: In: Proceedings of the Combustion Institute, 38, Elsevier Ltd, 2021, pp. 4757–4765, https://doi.org/10.1016/j.proci.2020.07.098.

[14] D.K. Kim, P.B. Sunderland, Fire ember pyrometry using a color camera, Fire Saf. J. 106 (2019) 88–93, https://doi.org/10.1016/j.firesaf.2019.04.006.

[15] J.H. Baldwin, P.B. Sunderland, Ratio pyrometry of emulated firebrand streaks, Fire Saf. J. (2023) 136, https://doi.org/10.1016/j.firesaf.2023.103746.

[16] J.A. De Beer, J.A. Alascio, S.I. Stoliarov, M.J. Gollner, Analysis of the thermal exposure and ignition propensity of a lignocellulosic building material subjected to a controlled deposition of glowing firebrands, Fire Saf. J. 135 (2023), https://doi.org/10.1016/j.firesaf.2022.103720.

[17] S.I. Stoliarov, R.E. Lyon, Thermo-kinetic model of burning for pyrolyzing materials, in: Fire Safety Science, 2008, pp. 1141–1152, https://doi.org/10.3801/IAFSS.FSS.9-1141.

[18] S.L. Manzello, A. Maranghides, W.E. Mell, Firebrand generation from burning vegetation, Int. J. Wildland Fire 16 (4) (2007) 458–462, https://doi.org/10.1071/WF06079.

[19] S.R. Turns, An Introduction to Combustion: Concepts and Applications, third ed., McGraw-Hill, 2012.

[20] I.T. Leventon, J. Li, S.I. Stoliarov, A flame spread simulation based on a comprehensive solid pyrolysis model coupled with a detailed empirical flame structure representation, Combust. Flame 162 (10) (2015) 3884–3895, https://doi.org/10.1016/j.combustflame.2015.07.025.

[21] J.V. Beck, Surface Heat Flux Determination Using an Integral Method, Nucl. Eng. Des. 7 (2) (1968) 170–178, https://doi.org/10.1016/0029-5493(68)90058-7.

[22] K. Strąk, B. Maciejewska, M. Piasecka, The heat transfer coefficient determination with the use of the Beck-Trefftz method in flow boiling in a minichannel, EPJ Web Conf. 180 (2018), 02099, https://doi.org/10.1051/epjconf/201818002099.

[23] ASTM E1354-23, Standard test method for heat and visible smoke release rates for materials and products using an oxygen consumption calorimeter, ASTM International, West Conshohocken, 2023.

[24] C.G. McCoy, J.L. Tilles, S.I. Stoliarov, Empirical Model of flame heat feedback for simulation of cone calorimetry, Fire Saf. J. 103 (2019) 38–48, https://doi.org/10.1016/j.firesaf.2018.11.006.

[25] F. Incorpera, D. De Witt, T. Bergman, A. Lavine, Fundamentals of Heat and Mass Transfer, sixth ed., John Wiley & Sons, Inc, 2007.

[26] F. Richter, B. Bathras, J. Barbetta Duarte, M.J. Gollner, The Propensity of Wooden Crevices to Smoldering Ignition by Firebrands, Fire Technol, 2022, https://doi.org/10.1007/s10694-022-01247-w. Published online.